Polymer Chemistry

Synthesis and characterization of a nematic fully aromatic polyester based on biphenyl 3,4'-dicarboxylic acid

Journal:	*Polymer Chemistry*
Manuscript ID	PY-ART-05-2019-000683.R1
Article Type:	Paper
Date Submitted by the Author:	19-Jun-2019
Complete List of Authors:	Heifferon, Katherine; Virginia Polytechnic Institute and State University, Department of Chemistry Spiering, Glenn; Virginia Polytechnic Institute and State University, Department of Chemistry Talley, Samantha; Virginia Tech University, Department of Chemistry, Macromolecules and Interfaces Institute Hegde, Maruti; Virginia Polytechnic Institute and State University, Department of Chemistry; University of North Carolina at Chapel Hill, Department of Applied Physical Sciences Moore, Robert; Virginia Tech, Department of Chemistry Turner, Richard; Virginia Tech, Macromolecules Innovation Institute Long, Timothy; Virginia Polytechnic Institute and State University, Department of Chemistry

Synthesis and characterization of a nematic fully aromatic polyester based on biphenyl 3,4'-dicarboxylic acid

Katherine V. Heifferon[a], Glenn A. Spiering[a], Samantha J. Talley[a], Maruti Hegde[a,b], Robert B. Moore[a], S. Richard Turner[a], and Timothy E. Long[a,*]

[a]*Macromolecules Innovation Institute, Department of Chemistry, Virginia Tech, Blacksburg, VA 24061*

[b]*Department of Applied Physical Sciences, University of North Carolina, Chapel Hill, NC, 27599-3050*

*To whom correspondence should be addressed. Email: telong@vt.edu. TEL: (540) 231-2480 FAX: (540) 231-8517

Keywords: polyester, liquid crystalline, melt polymerization, bibenzoate

Abstract:

Melt acidolysis polymerization of hydroquinone with a kinked monomer, biphenyl 3,4'-bibenzoate, afforded the synthesis of a novel liquid crystalline polymer (LCP), poly(*p*-phenylene 3,4'-bibenzoate) (poly(HQ-3,4'BB)). Selection of hydroquinone diacetate (HQ_a) or hydroquinone dipivilate (HQ_p) facilitated either a tan or white final polymer, respectively. ^{1}H NMR spectroscopy confirmed consistent polymer backbone structure for polymers synthesized with either derivative of hydroquinone. Poly(HQ-3,4'BB) exhibited an onset of weight loss at about 480 °C, similar to commercially available Vectra® LCP. Differential scanning calorimetry (DSC) and dynamic mechanical analysis (DMA) revealed a glass transition temperature (T_g) of 190 °C and an isotropic temperature (T_i) near 330 °C. The observation of a melting temperature (T_m) depended upon the thermal history of the polymer. Wide-angle X-ray scattering (WAXS) and polarized optical microscopy (POM) confirmed the formation of a nematic glass morphology after quench-cooling from the isotropic state. Subsequent annealing at 280 °C or mechanical deformation induced crystallization of the polymer. Rheological studies demonstrated similar shear thinning behavior for poly(HQ-3,4'BB) and Vectra® RD501 in the power law region at 340 °C. Zero-shear viscosity

measurements indicated that HQ_a afforded higher melt viscosities after identical polymerization conditions relative to HQ_p, suggesting higher molecular weights.

Introduction:

Thermotropic liquid crystalline polyesters (LCPs) represent a unique field of high-performance polymers with properties that enable electronic and automotive parts, high strength fibers, and stainless-steel replacements in the medical industry. These applications demand a complement of high thermal stability, dielectric strength, and chemical resistance.[1-4] Thermotropic LCPs exhibit anisotropic ordering when heated above the melting temperature, transitioning the morphology into a LC phase. This LC phase exhibits various degrees of translational and orientational order that reside between 3D crystallinity and a completely amorphous melt (isotropic).[4, 5] The LC mesophase facilitates enhanced levels of chain orientation during fiber formation, as well as drastic viscosity reductions under shear.[6] As a result of these beneficial properties, melt processing and polymerization often occurs in the presence of a LC phase, between the melting temperature (T_m) and the isotropic temperature (T_i), commonly referred to as the mesogenic window.

Small molecule liquid crystals, originally discovered by an Austrian botanist in 1888, often comprise rod- or disk-like shapes synthesized from aromatic rigid structures with an aspect ratio (length/diameter ratio) of ~ 6.[5, 7] In 1956, Flory hypothesized that incorporation of these small molecules into a polymer could impart LC properties to polymers.[8] The incorporation of the LC monomer typically occurs through polymerization into the backbone (main-chain) or incorporation as a pendant unit (side-chain).[5] Polyesters primarily utilize main-chain structures, and early patents in this field focus on acidolysis polymerization to synthesize polymers with fully aromatic backbones (polyarylates), such as the commercially available polymer Vectra®.[9-11]

Homopolymers of these rigid linear molecules, such as poly(*p*-phenylene terephthalate) or poly(*p*-hydroxybenzoic acid), resulted in very high melting temperatures (> 600 °C), rendering them improcessable with the exception of forging techniques.[12-14] Efforts to reduce T_m and improve processability focused on random copolymerization to disrupt translational symmetry. The focus on symmetrical aromatic comonomers (*para*: 180° bond angle) afforded the reduction in T_m while maintaining a stable LC phase, broadening the mesogenic window. In contrast, asymmetric or "kinked" aromatic comonomers (*meta*: 120° bond angle), although effectively reduce the T_m, often result in destabilization of the LC phase, which was attributed to disruption of chain linearity.[4, 13, 15] The linearity of the polymer plays an important role in the stability of the LC phase as a reduction of linearity results in decreasing the polymer aspect ratio (persistence length/diameter ratio), which needs to exhibit a value of > 6 to achieve a LC phase. As a result, homopolymers such as poly(*p*-phenylene isophthalate) or poly(*m*-hydroxybenzoic acid) do not exhibit LC properties despite their rigidity due to loss of rectilinearity.[4, 13, 16] Although exchanging an aromatic unit in the backbone with a flexible aliphatic spacer also reduces T_m, the thermal stability of polymer is compromised, as demonstrated in the earlier literature.[17-19]

In this manuscript, we describe the synthesis and characterization of a novel kinked polymer, poly (*p*-phenylene 3,4' bibenzoate) (poly(HQ-3,4'BB)). This wholly aromatic homopolymer is derived from biphenyl 3,4'-dicarboxylic acid (3,4'BB), which is the regioisomer of the common mesogenic monomer biphenyl 4,4'-dicarboxylic acid. Previous copolymerization of 4,4'BB based semi-aromatic polymers with 3,4'BB afforded a range of polymer morphologies from LC to amorphous with a trend of reduced melting temperatures upon increased incorporation of 3,4'BB.[19] In contrast to previous kinked homopolymers such isophthalates, the biphenyl unit of 3,4'BB forms a longer kinked structure, which facilitates formation a nematic mesophase and

limits polymer crystallization. This manuscript describes the first instance, to the best of our knowledge, of a fully aromatic homopolyester without pendant substituents that achieves LC behavior over an accessible temperature window for melt processing.

Experimental:

Materials.

Dimethyl 3,4'-biphenyldicarboxylate (dimethyl 3,4'-bibenzoate: 3,4'BB), Vectra® A950, and Vectra® RD501 samples were generously provided by ExxonMobil and used as received. Hydroquinone (HQ) (Sigma-Aldrich, ≥ 99%) and hydroquinone diacetate (HQ_{dac}) (Sigma-Aldrich, 98%) were recrystallized from ethanol (EtOH) (Decon Labs, 200 proof). Pivalic anhydride, also known as trimethylacetic anhydride, (Acros Organics, 99%), chloroform-*d* (*CDCl*$_3$) (Cambridge Isotope Laboratories, 99.8% atom D), trifluoroacetic acid-*d* (*d*-TFA) (Sigma-Aldrich, 99.5% atom D), dimethyl sulfoxide-d_6 (*DMSO-d*$_6$) (Cambridge Isotope Laboratories, 99.9% atom D), tetrahydrofuran (THF) (Fisher Chemical), and sodium hydroxide (NaOH) (Fisher Chemical) were used as received.

Analytical Methods.

A Varian Unity 400 at 400 MHz (23 °C) generated the ^{1}H and ^{13}C nuclear magnetic resonance (NMR) spectra of the monomers, in $CDCl_3$ and DMSO-d_6, and the polymer required *d*-TFA. A TA Instruments Q50 thermogravimetric analyzer (TGA), under constant N_2 flow, afforded the weight loss profile of the polymers during a ramp from 25 to 600 °C with a rate of 10 °C/min. A heat/cool/heat cycle using a rate of 10 °C/min, 100 °C/min, and 10 °C/min, respectively, on a TA Instruments Q1000 differential scanning calorimeter (DSC) with a 50 mL/min nitrogen flow, revealed the thermal transitions for the polymer. Indium (T_m = 156.60 °C) and zinc (T_m = 419.47 °C) standards calibrated the instrument prior to analysis. Data analysis occurred on the second heat

cycles using the inflection point of the T_g and the maximum of the T_i and T_m. Compression molding of the polymers utilized a sandwich of aluminum plates, Kapton® sheets coated with a Rexco Partall® Power Glossy Liquid mold release agent, and 400 μm thick stainless-steel shims between which the samples were placed. Heating above the T_i of the polymer at 340 °C generated films upon molding and an immediate quench in an ice bath quickly cooled the sample. Dynamic mechanical analysis (DMA) utilized an oscillatory amplitude of 15 μm, a frequency of 1 Hz, and a static force of 0.01 N while in tension mode. The TA Instruments Q800 DMA used a heating rate of 3 °C/min until reaching 300 °C, and subsequently the sample was rapidly cooled to room temperature prior to restarting the run. Analysis of the DMA measurement occured on the second heat and maximum of the tan delta afforded the T_g of the polymers.

Wide-angle X-ray scattering (WAXS) experiments were performed using a Rigaku S-Max 3000 3 pinhole SAXS system, equipped with a rotating anode emitting X-rays with a wavelength of 0.154 nm (Cu Kα). The sample-to-detector distance was 110 mm and the q-range was calibrated using a silver behenate standard. Two-dimensional diffraction patterns were obtained using an image plate with an exposure time of 1 h. WAXS data were analyzed using the SAXSGUI software package to obtain radially integrated WAXS intensity versus the scattering vector, 2θ, where $q=(4\pi/\lambda)\sin(\theta)$, θ is one half of the scattering angle and λ is the wavelength of X-ray. Polarized optical microscopy (POM) was performed by placing the samples between crossed polarizers of a Nikon LV100 Eclipse optical microscope equipped with a Linkham TMS 94 hot stage and a Nikon DXM1200 digital camera. Samples were pressed between glass slides after heating past the T_i and cooled at an approximate rate of either 10 °C/min or 75 °C/min. Melt rheology was performed on a TA instruments DHR-2 rheometer at 340 °C using a 1.25% strain with an 8 mm disposable parallel-plate geometry under N_2 flow. A hole punch generated circular

disks of the sample from a compression molded film, which were stacked 8 tall on the bottom geometry. The sample was heated to 340 °C then compressed together by lowering the top geometry into place. The linear viscoelastic region was determined prior to each frequency sweep using a strain sweep from 0.01 to 10% oscillatory strain at 1 rad/s in order to guarantee melding of the films. Frequency sweeps ranging from 1 to 100 rad/s afforded complex viscosity values and standard deviations from a minimum of three runs. Sample nomenclature comprises poly(HQ_a-3,4'BB) or poly(HQ_p-3,4'BB) where **a** and **p** refer to the use of acetylated or pivilated hydroquinone, respectively. The added identifier poly(HQ-3,4'BB): **X** min vac refers to the length of time of the vacuum stage during the polymers (X = 1, 30, or 60 min).

Synthesis of biphenyl 3,4'-dicarboxylic acid.

Dimethyl-3,4' bibenzoate (3,4'BB) (39.94 g, 0.148 mol) refluxed for 24 h in 400 mL of a 1M sodium hydroxide solution of 1:1 DI water:THF based on previous literature (**Scheme S1)**.[20] Filtration removed unreacted 3,4'BB, subsequent rotary evaporation removed the remaining THF. The final product, 3,4'BB-COOH, precipitated from the remaining aqueous solution upon the addition of concentrated HCl. Filtration and rinsing with distilled water neutralized the product, which was dried *in vacuo* at 120 °C overnight to remove residual water, resulting in a fine white powder (34.69 g, 97% yield).

^{1}H NMR (400 MHz, DMSO-d_6): δ 13.12 (s, 2H), 8.24 (s, 1H), 8.05(d, 2H), 7.99 (d, 2H), 7.84 (d, 2H), and 7.64 (t, 1H) ppm.

^{13}C NMR (400 MHz, DMSO-d_6): δ 167.51, 143.73, 139.78, 132.03, 131.73, 130.51, 129.90, 129.44, 127.96, and 127.36 ppm.

Melting Point (DSC): 103 °C

Synthesis of hydroquinone dipivilate.

Hydroquinone (5.1g, 0.046 mol) and pivalic anhydride (20 mL, 0.135 mol) were weighed into a dry 100-mL, round-bottomed, flask equipped with a t-neck adaptor, distillation tube, a round-bottomed collection flask, glass stir-rod adaptor, mechanical stir-rod, and an overhead mechanical stirrer. Evacuation and back-filling of the reaction vessel occurred three times with N_2 and a vacuum pump to ensure an inert atmosphere. Heating the reaction at 170 °C under constant N_2 flow removed the pivalic acid condensate into a distillation flask (**Scheme S2)**. According to thin layer chromatography, the reaction achieved full conversion after 1 h, which prompted cooling to room temperature. The product crystallized from the resulting solution upon cooling, and filtration from the remaining pivalic anhydride and further washes with EtOH facilitated purification. A white crystalline solid resulted after drying the resulting product, hydroquinone dipivilate (HQ_{dpv}), *in vacuo* overnight at 100 °C.

^{1}H NMR (400 MHz, $CDCl_3$): δ 7.04 (s, 4H) and 1.33 (s, 18H) ppm.

^{13}C NMR (400 MHz, $CDCl_3$): δ 176.91, 148.29, 122.20, 39.04, and 27.09 ppm

Melting Point (DSC): 104 °C

Synthesis of poly(*p*-phenylene 3,4'-bibenzoate).

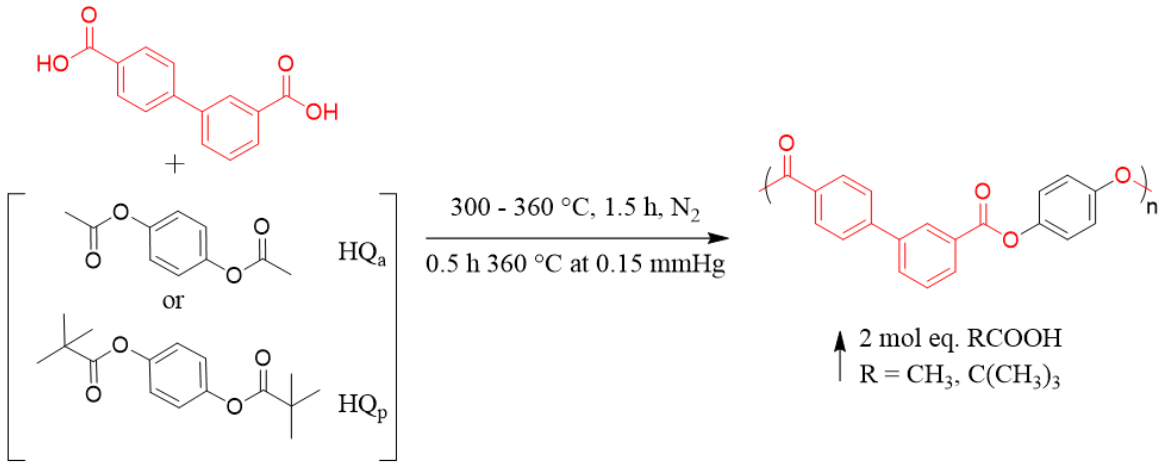

Scheme 1. Synthesis of poly(hydroquinone-3,4'-bibenzoate) through acidolysis polycondensation utilizing either hydroquinone diacetate (poly(HQ_a-3,4'BB)) or hydroquinone dipivilate (poly(HQ_p-3,4'BB)).

Acidolysis polymerization afforded a liquid crystalline, fully aromatic, polymer as illustrated in **Scheme 1**.[10, 11, 21] 3,4'BB-COOH (6.237 g, 0.026 mol) and either HQ_a (5 g, 0.026 mol) or HQ_p (7.167 g, 0.026 mol) were weighed into an oven dried, 100-mL, round-bottomed flask. The reactor comprised a t-neck adaptor, distillation tube with a 100-mL round-bottomed collection flask, glass stir-rod adaptor, mechanical stir-rod, and an overhead mechanical stirrer. Evacuation and back-filling of the reaction set-up with vacuum and N_2 three-times ensured an inert atmosphere. Heating the reaction from 300 to 360 °C under N_2 flow for 1.5 h afforded a homogenous clear melt. Finally, application of reduced pressure (0.15 mmHg) for 0.5 h at 360 °C produced a highly viscous tan or white polymer, as illustrated in **Figure 1**, which was utilized without further purification.

For the polymerization studies, three equivalent reactions using HQ_a and HQ_p separately (6 total) were stopped after different lengths of time under vacuum during the final stage of the reaction (1 min, 30 min, or 60 min). Rheological properties of the resulting polymers were measured without further purification.

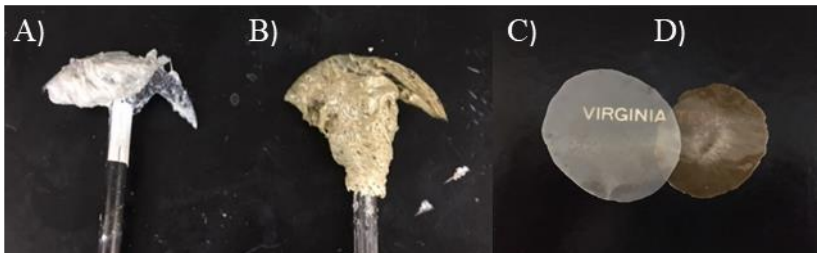

Figure 1. Poly(hydroquinone-3,4'-bibenzoate) before (A/B) and after (C/D) compression molding utilizing hydroquinone dipivilate (A/C) or hydroquinone diacetate (B/D).

Results and Discussion:

Scheme 1 illustrates the polymerization of poly(*p*-phenylene 3,4' bibenzoate) (poly(HQ-3,4'BB) utilizing an acidolysis strategy. Hydrolysis of dimethyl 3,4'-bibenzoate generated the diacid derivative using procedures from Stock et al. earlier, to enable the acidolysis

polymerization.[20] ^{1}H and ^{13}C NMR spectroscopy confirmed the structure of this monomer after purification. For the second monomer, this work investigated the two derivatives of hydroquinone: hydroquinone diacetate (HQ_a) and hydroquinone dipivilate (HQ_p). Early patents and publications, which described fully aromatic LCPs, demonstrated success through the *in-situ* generation of these hydroquinone derivatives during the polymerization. This synthesis progressed through a one-pot reaction of the diacid, diphenol, and acetic/pivalic anhydride.[9-11, 22] While this synthetic pathway represents a more commercially viable polymerization method to generate LCPs, pre-acetylated/pivilated hydroquinone enabled consistent polymerization conditions throughout all reactions studied. This strategy guaranteed accurate stoichiometries of acetylated/pivilated phenolic monomers at the onset of the polymerization and ensured identical reaction times and temperatures for all polymerizations.[7, 21, 23]

Recrystallization of the commercially available hydroquinone diacetate from EtOH afforded a pure starting material. Synthesis of hydroquinone dipivilate occurred in a solvent-free reaction between HQ and pivalic anhydride, similar to *in-situ* polymerization conditions. The synthetic method utilized 3 eq. excess pivalic anhydride, which generated pivalic acid upon reaction with hydroquinone at 170 °C. The high temperature and nitrogen flow facilitated removal of the by-product, driving the reaction toward completion. Upon cooling, HQ_p recrystallized from the remaining pivalic anhydride and afforded a pure product after rinsing with EtOH. ^{1}H and ^{13}C NMR spectroscopy confirmed the structure and purity of the monomer prior to polymerization.

Acidolysis polymerization generated poly(HQ-3,4'BB) using a high temperature heating ramp from 300 to 360 °C, and the monomers maintained a transparent homogenous melt. During the final step of the reaction, the application of vacuum drove the reaction to high conversion and achieved a high viscosity polymer melt, which wrapped the metal stir-rod. Due to the high

viscosity of the final polymer, as well as the subsequent removal of a large amount of condensate (acetic acid or pivalic acid), the application of vacuum resulted in foaming, which is common for these polymerizations.[24] ^{1}H NMR spectroscopy in a 1:1 mixture of $CDCl_3$:d-TFA (**Figure S4**) confirmed the structure of poly(HQ_a-3,4'BB) and poly(HQ_p-3,4'BB), verifying insignificant backbone differences between the polymers due to the different condensate. The two polymers exhibited very limited solubility in standard solvents, such as THF and $CHCl_3$, preventing the use of size exclusion chromatography to determine molecular weights. However, ductile films through compression molding suggested the formation of polymers above the molecular weight of entanglement.[25-28]

Hall et al. previously studied ketene formation in the model compounds *p-tert*-butyl phenyl acetate and *p-tert*-butyl phenyl pivilate. This study linked ketene production with color-forming side-reactions, which result in the persistent tan color observed in most fully aromatic LCPs synthesized through high temperature acidolysis.[29] Hall also found that the lack of an α-hydrogen on the pivilate compound prevented ketene formation at high temperatures, therefore reducing color formation with respect to the acetate.[29] Comparison of HQ_a and HQ_p in the polymerization of poly(HQ-3,4'BB) corroborated this earlier study, resulting in a considerably less colored polymer from the pivilated monomer, as illustrated in **Figure 1.** These side reactions, which cause color formation, occur at concentrations below the detection limit of NMR spectroscopy and therefore were not analyzed through this method.

Thermal Characterization:

Thermogravimetric analysis characterized the thermal stability of the polymer as a function of temperature, as illustrated in **Figure 2.** Poly(HQ_a-3,4'BB) and poly(HQ_p-3,4'BB) exhibited

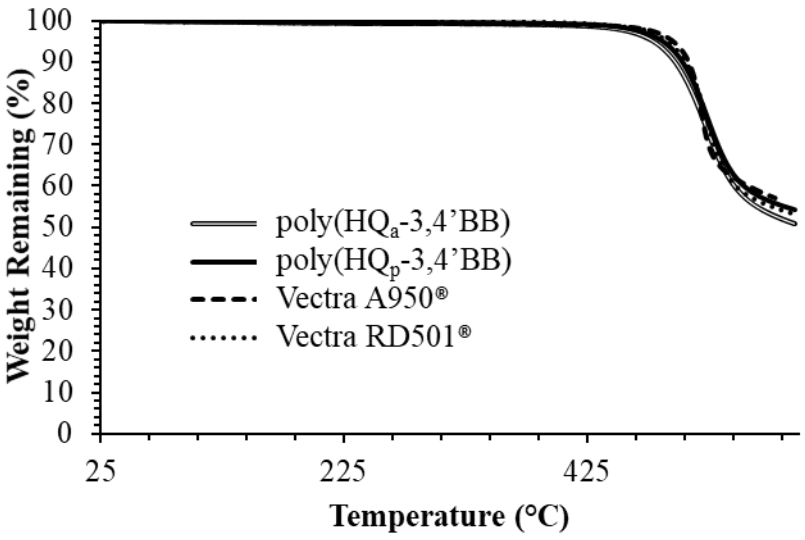

Figure 2. Thermogravimetric analysis of poly(HQ_a-3,4'BB), poly(HQ_p-3,4'BB), and two unfilled Vectra® industrial standards.

one-step weight loss profiles with overlapping $T_{d,5\%}$ values of 480 and 487 °C, respectively. These polymers exhibit nearly identical weight-loss profiles to the two unfilled industrial standards, Vectra® A950 and Vectra® RD501. Vectra® A950's structure consists of a comonomer composition of 6-hydroxy-2-naphthoic acid (HNA) and para-hydroxybenzoic acid (*p*-HBA). Vectra® RD501 consists of four different monomeric units (HNA, *p*-HBA, terephthalic acid (TA),

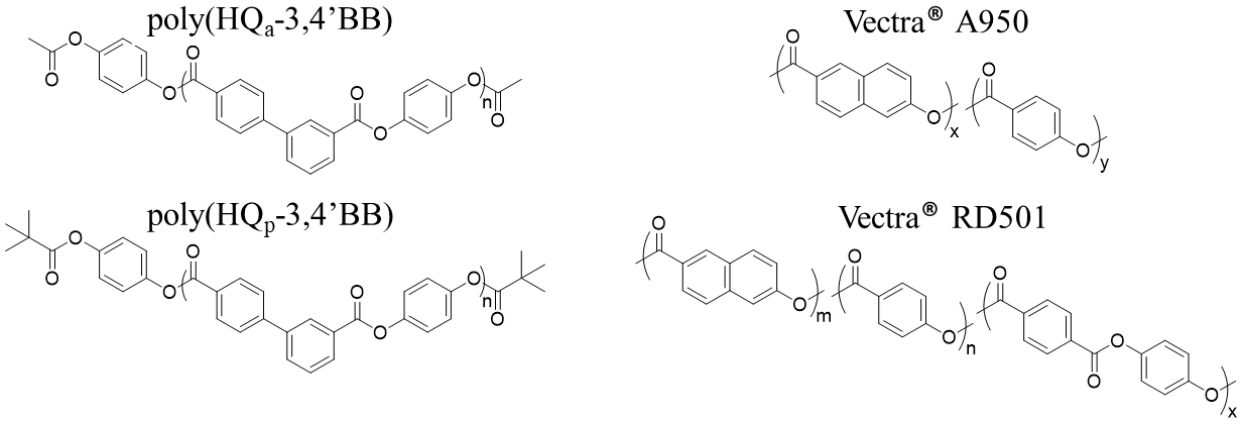

Figure 3. Chemical structures of polymers characterized demonstrating the differences between the lab made poly($HQ_{a/p}$-3,4'BB) and the industrial standards Vectra® A950/RD501**.**

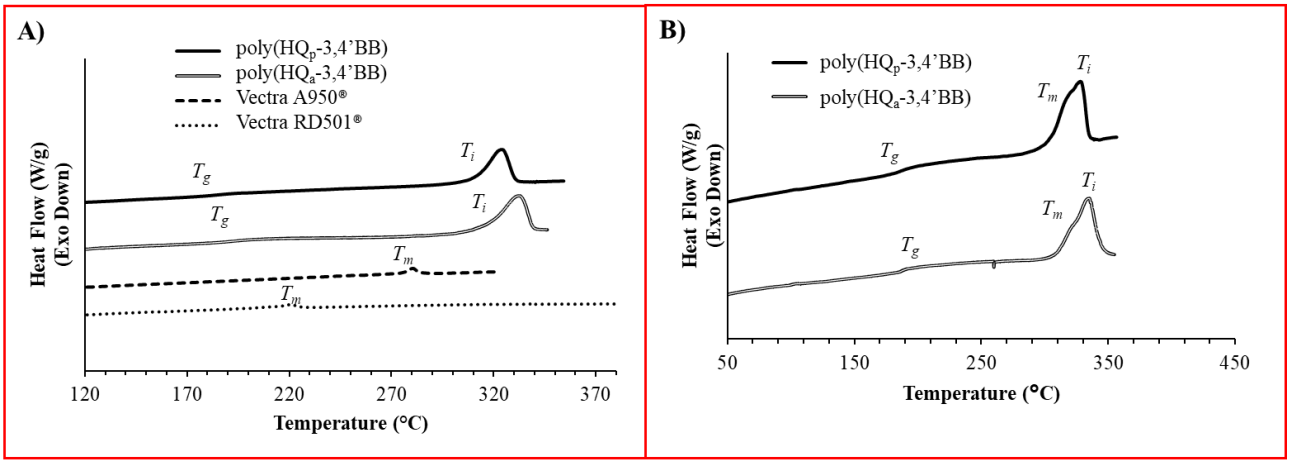

Figure 4. Second heating traces in DSC after A) quench cool or B) slow cool for poly(HQ$_a$-3,4'BB) and poly(HQ$_p$-3,4'BB).

and HQ).[30-32] The differences between the random copolymer structures of Vectra® and the lab made homopolymers, poly(HQ$_{a/p}$-3,4'BB), are further illustrated in **Figure 3**. The Vectra® and poly(HQ-3,4'BB) samples exhibited an insignificant difference between their char yield or the $T_{d,5\%}$ due to the similar bond stability in these backbone structures.

Differential scanning calorimetry revealed the thermal transitions for these four polymers, as illustrated in **Figure 4A** and **Table 1**. The DSC of Vectra® A950 and Vectra® RD501 revealed an endothermic transition at 280 and 220 °C, respectively, with ΔH_m of 1.63 and 1.82 J/g. These transitions correspond to the T_m of these polymers as the polymer transitions from a semi-crystalline to a nematic morphology. The T_i was not observed for these polymers as it resides above the degradation temperature, resulting in processing and polymerization occurring in the desirable nematic state.[33] DSC did not reveal T_g's for these two standards, but references identify these values as 93 and 112 °C, respectively.[32] In sharp contrast to the Vectra® samples, both poly(HQ$_a$-3,4'BB) and poly(HQ$_p$-3,4'BB) exhibited obvious T_g's at 191 °C and 188 °C, respectively, which was within error of each other with a ΔC_p of 0.05 W/g. The more obvious T_g

Table 1. Thermal characterization of poly(HQ_a-3,4'BB), poly(HQ_p-3,4'BB), and two Vectra® standards utilizing TGA and DSC.

Sample	$T_{d,5\%}$ (°C)	Char yield (%)	T_g (°C)	ΔC_p (W/g)	T_m (°C)	ΔH_m (J/g)	T_i (°C)	ΔH_i (J/g)
Poly(HQ_a-3,4'BB)	480	51	191	0.05	320[a]	N/A	332	26.7
Poly(HQ_p-3,4'BB)	487	54	188	0.05	315[a]	N/A	324	20.4
Vectra A950	496	57	93[b]	0.03[b]	280	1.63	> 500[b]	N/A
Vectra RD501	491	53	112[b]	N/A	220	1.82	> 500[b]	N/A

[a] Only observed after slow cool at 10 °C/min
[b] Value determined from reference materials
N/A indicates unable to measure value accurately

possibly correlates with a higher amorphous content in the novel polymer due to the kinked structure relative to the more linear structure of Vectra®.[34]

Both poly(HQ_a-3,4'BB) and poly(HQ_p-3,4'BB) also revealed one large endothermic transition each at 332 and 324 °C during the heat cycle following a quench-cool (100 °C/min from 360 °C) in the DSC, as illustrated in **Figure 4A**. In contrast to the Vectra® samples, this transition represented the T_i (LC to isotropic transition) with a larger ΔH_i of 26.7 and 20.4 J/g, respectively. In contrast, processing the polymer through a slow cool (10 °C/min) from 360 °C facilitated the formation of a shoulder on the T_i at 315 °C and 320 °C, respectively, during the following heat cycle (**Figure 4B**). This new transition presumably represents the T_m of this LC polymer. This overlap of the peaks inhibited accurate measurement of the enthalpy values for this transition. The inability to observe the T_m under quench-cooling suggests that this system forms a LC glass, which hinders the formation of 3D crystalline packing structure while maintaining a LC mesophase below the T_g. This would significantly broaden the mesogenic window of the polymer. Polarized optical microscopy and WAXS further probed the morphological changes to determine LC phase and crystallization properties.

Morphological Characterization:

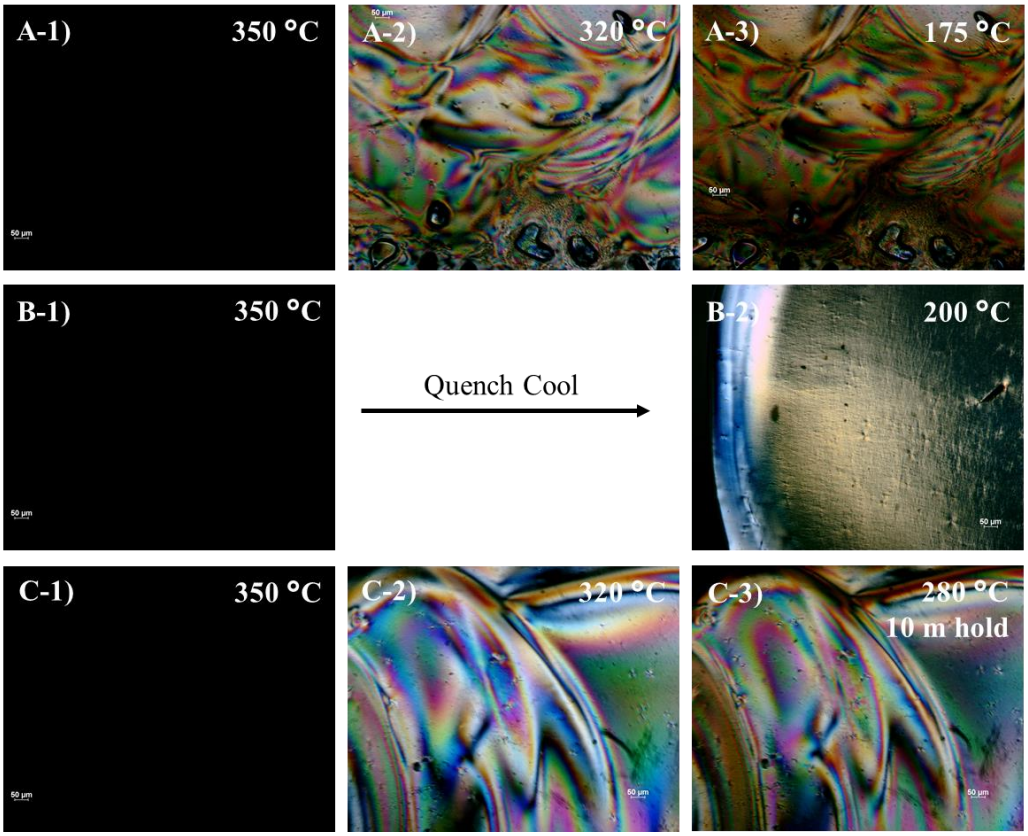

Figure 5. Polarized optical microscopy of poly(HQ_p-3,4'BB) reveals birefringence with schlieren texture under different thermal treatments. A) Cooling at 10 °C/min from isotropic B) Cooling at 75 °C/min from isotropic C) Cooling at 10 °C/min from 350-280 °C then isotherm for 10 m.

Polarized optical microscopy facilitated the initial characterization of the morphology of poly(HQ-3,4'BB). The lowest viscosity sample from the molecular weight study, poly(HQ_p-3,4'BB): 1 min vac, enabled significant flow between the glass slides forming a thin section. This allowed the formation of a clear image of the LC phase. Heating the polymer above the endothermic transition to 350 °C formed an isotropic melt without birefringence. Cooling the sample at a rate of 10 °C/min facilitated the transition into a birefringent texture at 320 °C, observed in **Figure 5A-2.** Cooling to 175 °C, below the T_g, maintained the same texture**.** Optical comparison of this texture to previous literature of other LCPs classifies the birefringence as a schlieren texture, common for nematic LC's.[35, 36] The images in **Figure 5B** represent a quench-cooled sample using a rate of 75 °C/min from isotropic (350 °C) to 200 °C. The study revealed

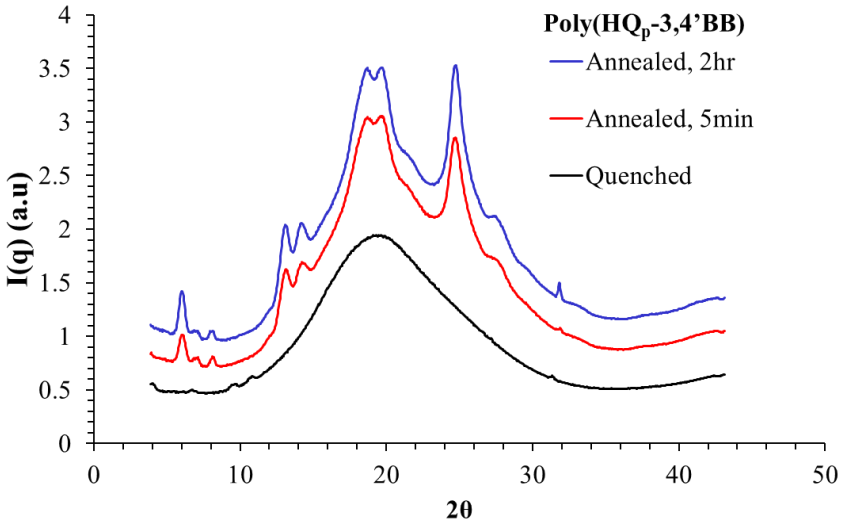

Figure 6. WAXS integration analysis of poly(HQ_p-3,4'BB) after different thermal history. Curves vertically shifted for clarity.

that the polymer possessed birefringence after quenching without an easily identifiable texture (**Figure 5B-2**). This confirms that quenching the sample does not eliminate LC phase resulting possibly in a LC glass. Slow cooling the sample from 350 °C to 280 °C, in **Figure 5C**, and subsequently holding for 10 min did not promote significant texture change as is often observed during crystallization.[4, 37] While this is contradictory to the DSC results, it was presumed that at a low % crystallinity, a change in texture may not be observed. Attempts to analyze higher molecular weight samples enabled the observation of birefringence below the T_i, but the high viscosity resulted in samples too thick for obvious LC textures (**Figure S5**). Even so, these samples did not demonstrate an obvious difference in texture between poly(HQ_a-3,4'BB) and poly(HQ_p-3,4'BB).

Performing WAXS on a compression molded film of poly(HQ_p-3,4'BB) after different thermal treatments verified the polarized optical microscopy. Rapidly cooling the initial compression molded film from the isotropic state (340 °C) in an ice bath provided a quench-cooled sample for analysis. The single diffuse scattering peak (**Figure 6 and 7**) indicates the absence of a 2D layer structure that often forms lamellar morphologies prevalent in smectic mesophases; the data also confirms the absence of the packing structure of crystalline domains.[38-40] The few minor

peaks occurring in the quenched film may indicate insufficient quenching of the thick film in comparison to the much thinner polarized optical microscopy sample. Upon heating the polymer film for 5 min at 280 °C, sharp angular reflections emerged at 5.2, 6.1, 13.1, 14.2, 18.6, 19.6, 24.6, and 31.7° 2θ indicative of a semi-crystalline morphology forming in the polymer film corroborating the secondary shoulder observed in the DSC analysis. These sharp reflections increased slightly in intensity after longer annealing times (2 h at 280 °C). This limited crystallinity may have hindered the observation of a textural change in the optical microscopy after 10 min of annealing. Attempts to orient the quench-cooled sample below the T_i (310 °C) resulted in strain-induced crystallization rather than orientation (**Figure S6**). While the crystallization during orientation limits the ability to confirm the mesophase morphology for the polymer, the observation of a schlieren texture using polarized optical microscopy highly suggests a nematic morphology.

From the overall morphological characterization, poly(HQ_p-3,4'BB) appears to form a nematic LC mesophase below the main endothermic transition, identified as the T_i. Processing the material through a quench-cool, imparts a LC glass morphology in which the LC mesophase exists below the T_g of the material without the presence of crystalline domains. Confirmation of the LC

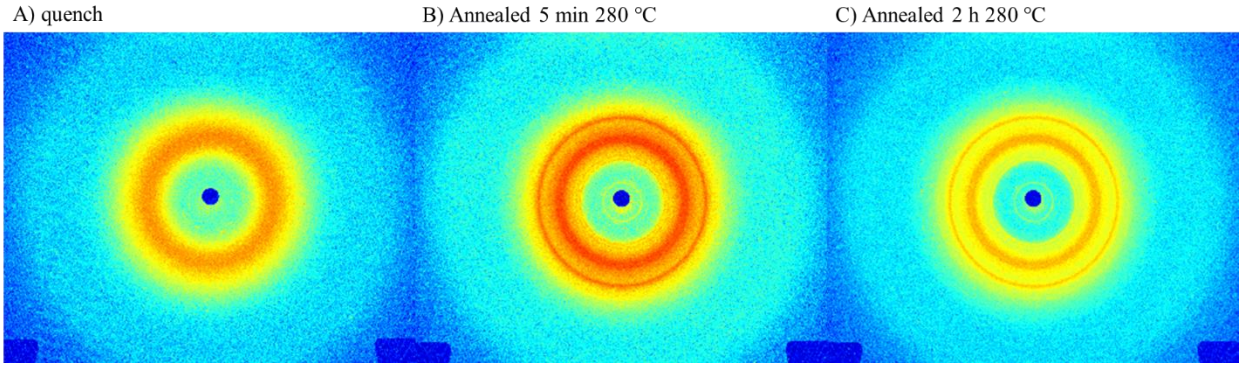

Figure 7. 2D WAXS profiles of poly(HQ_p-3,4'BB) after different thermal history. A) quench cooled from isotropic B) quenched film annealed for 5 m at 280 °C C) quenched film annealed for 2 h at 280 °C.

glass was achieved with the observation of a birefringent texture after a quench cool. Polarized optical microscopy coupled with room temperature diffraction patterns (**Figure 6 and 7a**), consisting of a single diffuse scattering peak centered about 20° 2θ, is typically indicative of an amorphous polymer. Both thermal treatments (annealing and slow cooling) and mechanical deformation promote crystallization of the polymer films. This crystallization results in a second endothermic transition, near the T_i, resulting in the commonly shown multipeak DSC curve for LC polymers. This crystallization remains consistent with other kinked non-LC fully aromatic polyesters, such as poly(*m*-HBA) and poly(IA-HQ), which exhibit semi-crystalline morphologies.[15] In contrast to these earlier examples, to the best of our knowledge this represents the first fully-aromatic polyester homopolymer that exhibits a stable LC mesophase without requiring copolymerization or pendant substituents from the backbone to achieve melt processability. The difference between these polymers lies in the longer kink structure of the biphenyl monomer which may increase the persistence length of the polymer fostering an aspect ratio within the required range for liquid crystallinity (>6).[8, 41] However, future work is necessary to confirm this hypothesis.

Thermomechanical Characterization:

Dynamic mechanical analysis (DMA) probed the thermomechanical properties of poly(HQ_a-3,4'BB). During the first heat cycle, the DMA heated the film under tension mode through the α-transition until 300 °C at which an increase in the modulus occurred and reached a maximum. Due to the temperature at which the maximum occurs, this is believed to be attributed to a combination of crystallization and improvement of the nematic ordering. Deconvolution of these two mechanisms will require further characterization. Quickly cooling the sample to room temperature and rescanning is depicted in **Figure 8.** The DMA curve exhibited a T_g at 208 °C,

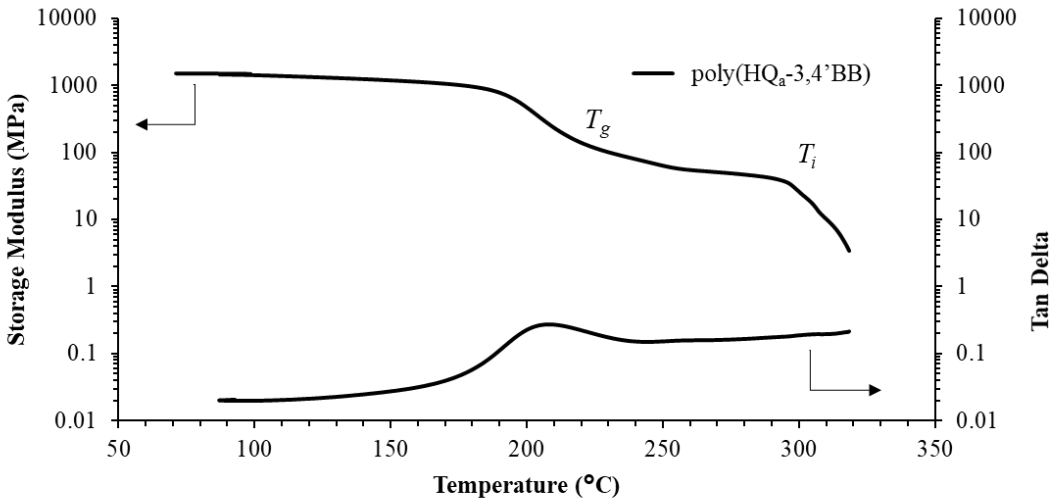

Figure 8. Dynamic mechanical analysis temperature ramp of poly(HQ_a-3,4'BB) at a frequency of 1 Hz.

slightly higher than the DSC value. The onset of flow began at 298 °C and continued until after the measured T_i (332 °C). Nematic LCPs commonly flow within the mesogenic window ($T_m - T_i$) allowing for polymerization and processing when an isotropic state cannot be achieved.[12] DMA of Vectra® A950exhibits the onset of flow near the T_m due to the semi-crystalline morphology.[42] This inhibition of flow below the T_i for poly(HQ-3,4'BB) presumably resulted from crystallization. Thus, poly(HQ-3,4'BB) achieves processability in the isotropic state at 340 °C, impossible for Vectra® which never achieves an isotropic state.

The importance of characterizing the viscous flow properties of LC polymers stems from the significant use of the shear thinning properties for LCPs. The power law coefficient represents a value for comparison of the shear thinning behavior of a polymer, expressed as n in **Equation 1**. This equation outlines the viscosity (η) change in the power law region of a polymer during melt rheology as a function of the consistency index (m) and shear rate (γ) to the power law coefficient minus 1. The values of n range from 0 to 1, where lower values result from steeper slopes (more significant shear thinning).

$$\eta = m(x)\gamma^{(n-1)} \quad (1)$$

The inhibition of flow below the T_i due to crystallization required melt rheology measurements at 340 °C. The experiment utilized a strain-sweep to determine the linear viscoelastic region then a frequency sweep from 0.1 to 100 rad/s. Power law scaling determined the exponent of the logarithmic viscosity slope from 1 to 10 Hz in the power law region, as illustrated in **Figure 9**. Vectra® RD501, has a power law coefficient of 0.14 at the same temperature (340 °C) as poly(HQ-3,4'BB), which falls within the nematic mesophase for this polymer. In comparison, poly(HQ_a-3,4'BB) and poly(HQ_p-3,4'BB) resulted in slightly higher values of 0.18 and 0.22, respectively, although these values are within the isotropic phase of these polymers. Although similar to Vectra®, this slight difference in shear thinning could be attributed to different morphologies for each polymer at 340 °C. The difference in shear thinning between poly(HQ_a-3,4'BB) and poly(HQ_p-3,4'BB) may result from the different end-groups or slight differences in polydispersity of the polymers. This characterization also revealed a significant difference between the zero-shear viscosities of poly(HQ_p-3,4'BB) and poly(HQ_a-3,4'BB). Due to the dependence of this value on

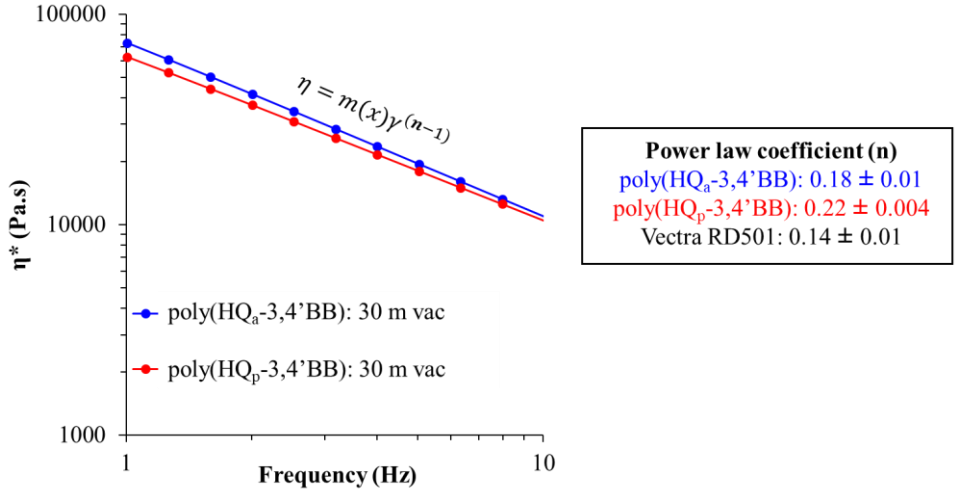

Figure 9. Viscosity profile of poly(HQ_a-3,4'BB) and poly(HQ_p-3,4'BB) at 340 °C within the power law region. Structural dependence of shear thinning characterized through analysis of power law coefficient.

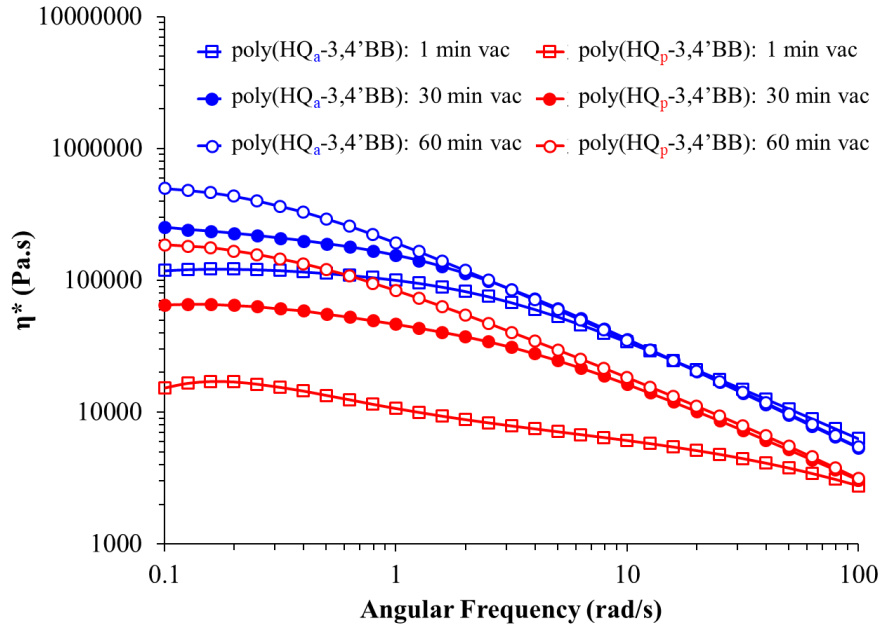

Figure 10. Frequency sweep at 340 °C with 1.25% strain of poly(HQ_a-3,4'BB) and poly(HQ_p-3,4'BB) polymers stopped at different % conversion during vacuum stage of polymerization.

molecular weight, a study was designed to probe the molecular weight growth of these two polymers.

Rheological study of molecular weight growth:

In order to probe the different molecular weight growth through the indirect measurement of zero-shear complex viscosity, six polymerizations of poly(HQ-3,4'BB) were performed (three utilizing HQ_a and three HQ_p). Consistent reaction scale, molar equivalents of HQ to 3,4'BB-COOH (1:1 mol eq.), and reaction times (with the exception of the vacuum stage) limited the errors occurring between the different reactions. As mentioned in the experimental section, stopping the three parallel reactions for HQ_a or HQ_p at different times in the vacuum stage (1 min, 30 min, and 60 min) enabled tracking of the molecular weight growth at different stages of the reaction. **Figure 10** displays the range of zero-shear viscosities achieved from the six polymer samples. The complex viscosity at 0.1 rad/s determined the zero-shear viscosity for each sample from triplicate runs, maintaining the same pre-shear treatment and instrument set-up to limit error. Plotting these

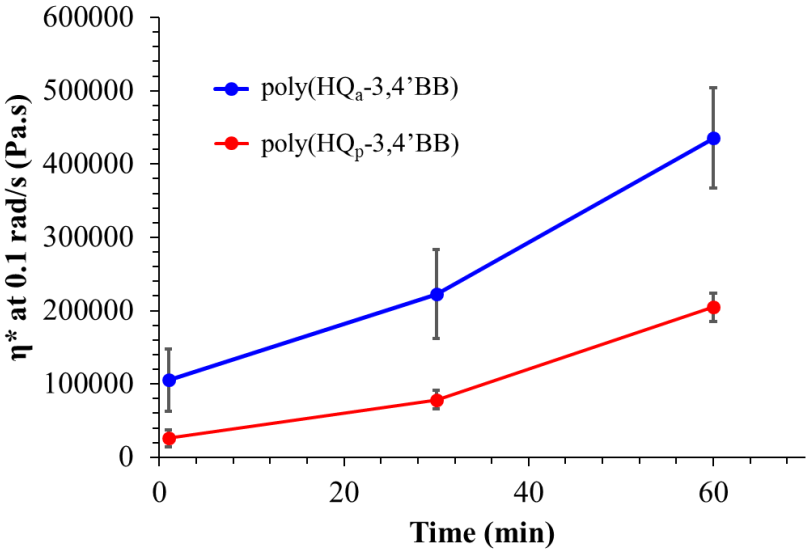

Figure 11. Comparison of the effects of length of time under vacuum during final polymerization on zero shear viscosity for poly(HQ_a-3,4'BB) and poly(HQ_p-3,4'BB) polymers.

two series in **Figure 11** as a function of vacuum time**,** enabled the observation that the zero-shear complex viscosity for the poly(HQ_a-3,4'BB) was consistently higher than poly(HQ_p-3,4'BB) with slightly higher slopes. This suggested that poly(HQ_a-3,4'BB) achieved higher molecular weight faster during the final stage of the reaction than poly(HQ_p-3,4'BB). The difference in condensate remains the only change between these two systems affecting molecular weight growth. The steric hinderance of ($C(CH_3)_3$) on the pivilate in comparison to acetate (CH_3) will result in slower conversion of the phenol to the mixed anhydride of the carboxylic acid slowing the molecular weight growth. Even so, depending on the color requirements for specific applications the white product achieved at the end when utilizing the poly(HQ_p-3,4'BB) could outweigh the slower reaction time to obtain the same molecular weight as poly(HQ_a-3,4'BB).

Conclusions:

Melt acidolysis polymerization afforded the synthesis of poly(HQ-3,4'BB), utilizing two different derivatives of hydroquinone: HQ_a and HQ_p. The variation in chemical structure of these monomers afforded lower coloring through use of HQ_p, however these polymers also exhibited

lower molecular weight. Structural analysis utilizing NMR spectroscopy confirmed that no significant difference in the polymer chemical structure occurred despite the condensate side-reactions causing a persistent color difference. Morphological characterization utilizing wide-angle x-ray scattering (WAXS) and polarized optical microscopy confirmed nematic morphology as well as limited crystallization under certain thermal and mechanical processing conditions. These results contradict previous understanding that kinked backbone structures inhibit the formation of a LC phase, presumably due to the longer biphenyl unit and its impact on the persistence length of the polymer. This LC polymer achieved comparable shear thinning results to the industrial standard, Vectra® RD501. This offers a competitive design for the synthesis of LC homopolymer without the necessity to complicate the structure through copolymerization in order to achieve processable temperature ranges. This material could be considered for a range of possible application in the areas of electronics and medical devices.

Funding:

This work is sponsored by ExxonMobil Chemical Company

Acknowledgments:

The authors thank Dr. Ryan Mondschein and Dr. Eliot Edling for insightful discussions throughout the project. The morphological characterization is supported by National Science Foundation under Grant No. DMR-1809291.

Notes:

The authors declare no competing financial interest

References:

1. A. M. Donald, A. H. Windle and S. Hanna, *Liquid crystalline polymers*, Cambridge University Press, Cambridge, 2nd edn., 2006.

2. A. H. Windle, in *Liquid Crystalline and Mesomorphic Polymers*, eds. V. P. Shibaev and L. Lam, Springer New York, New York, NY, 1994, DOI: 10.1007/978-1-4613-8333-8_2, pp. 26-76.
3. M. G. Dobb and J. E. McIntyre, in *Liquid Crystal Polymers II/III*, ed. N. A. Platé, Springer Berlin Heidelberg, Berlin, Heidelberg, 1984, DOI: 10.1007/3-540-12994-4_2, pp. 61-98.
4. T. Chung, *Thermotropic liquid crystal polymers: thin-film polymerization, characterization, blends, and applications*, Technomic Pub. Co, Lancaster, Pa, 2001.
5. K. V. Heifferon and T. E. Long, in *Liquid Crystalline Polymers: Synthesis, Properties, and Applications*, ed. V. Mittal, Central West Publishing, Australia, 2018, ch. 7, pp. 205-255.
6. W. G. Perkins, A. M. Marcelli and H. W. Frerking, *J. Appl. Polym. Sci.*, 1991, **43**, 329-349.
7. C. Tai-Shung, *Polymer Engineering & Science*, 1986, **26**, 901-919.
8. P. J. Flory, in *Recent Advances in Liquid Crystalline Polymers*, ed. L. L. Chapoy, Springer Netherlands, Dordrecht, 1985, DOI: 10.1007/978-94-009-4934-8_6, pp. 99-103.
9. *United States Pat.*, US 4,161,470, 1977.
10. *United States Pat.*, US4169933 A, 1979.
11. *United States Pat.*, US 4,522,974, 1985.
12. W. J. Jackson, *British Polymer Journal*, 1980, **12**, 154-162.
13. Z. Yerlikaya, S. Aksoy and E. Bayramli, *J. Appl. Polym. Sci.*, 2003, **90**, 3260-3269.
14. J. Economy and Z. Parkar, in *100+ Years of Plastics. Leo Baekeland and Beyond*, American Chemical Society, 2011, vol. 1080, ch. 7, pp. 93-103.
15. Z. Yerlikaya, S. Aksoy and E. Bayramli, *Journal of Macromolecular Science, Part A*, 2006, **43**, 433-447.
16. A. B. Erdemir, D. J. Johnson and J. G. Tomka, *Polymer*, 1986, **27**, 441-447.
17. M. Tokita and J. Watanabe, *Polym. J*, 2006, **38**, 611-638.
18. J. Watanabe and M. Hayashi, *Macromolecules*, 1988, **21**, 278-280.
19. K. V. Heifferon, R. J. Mondschein, S. J. Talley, R. B. Moore, S. R. Turner and T. E. Long, *Polymer*, 2019, **163**, 125-133.
20. M. Lammert, M. T. Wharmby, S. Smolders, B. Bueken, A. Lieb, K. A. Lomachenko, D. D. Vos and N. Stock, *Chem. Commun.*, 2015, **51**, 12578-12581.
21. A. F. Orifici, E. M. Vallés, R. O. Garay and R. W. Lenz, *Polymer*, 1996, **37**, 4357-4363.
22. J. N. Huang, J. P. Leblanc and H. K. Hall, *J. Polym. Sci. Pol. Chem.*, 1992, **30**, 345-354.
23. W. J. Jackson and H. F. Kuhfuss, *Journal of Polymer Science: Polymer Chemistry Edition*, 1976, **14**, 2043-2058.
24. M. Bakir, J. L. Meyer, J. Economy and I. Jasiuk, *Macromolecules*, 2016, **49**, 6489-6496.
25. A. M. Nelson, G. B. Fahs, R. B. Moore and T. E. Long, *Macromol. Chem. Phys.*, 2015, **216**, 1754-1763.
26. F. E. Arnold and R. L. Van Deusen, *Macromolecules*, 1969, **2**, 497-502.
27. J.-M. Yeh, S.-J. Liou, C.-Y. Lai, P.-C. Wu and T.-Y. Tsai, *Chem. Mater.*, 2001, **13**, 1131-1136.
28. Z. Dobkowski, *Rheol. Acta*, 1995, **34**, 578-585.
29. J.-P. Leblanc, J. Huang, A. B. Padias and H. K. Hall, *J. Polym. Sci., Part A: Polym. Chem.*, 1992, **30**, 2321-2332.
30. P. K. Mandal, S. K. Siddhanta and D. Chakraborty, *J. Appl. Polym. Sci.*, 2012, **124**, 5279-5285.
31. M. K. Kundu, P. Pal, G. Hatui, C. K. Das and S. S. Kalra, *J Polym Res*, 2015, **22**, 29.

32. W. N. Kim and M. M. Denn, *J. Rheol.*, 1992, **36**, 1477-1498.
33. J. Blackwell and A. Biswas, in *Developments in Oriented Polymers—2*, ed. I. M. Ward, Springer Netherlands, Dordrecht, 1987, DOI: 10.1007/978-94-009-3427-6_5, pp. 153-197.
34. G. G. Odian, *Principles of polymerization*, Wiley, New York, 1991.
35. Y. Wang, G. Lu, W. Wang, M. Cao, Z. Luo, N. Shao and B. Wang, *e-Polymers*, 2017, **17**, 199-207.
36. Y. Tian, E. Akiyama and Y. Nagase, *J. Mater. Chem.*, 2003, **13**, 1253-1258.
37. C. H. R. M. Wilsens, B. A. J. Noordover and S. Rastogi, *Polymer*, 2014, **55**, 2432-2439.
38. Y. S. Hu, D. A. Schiraldi, A. Hiltner and E. Baer, *Macromolecules*, 2003, **36**, 3606-3615.
39. Y. S. Hu, R. Y. F. Liu, D. A. Schiraldi, A. Hiltner and E. Baer, *Macromolecules*, 2004, **37**, 2128-2135.
40. Y. S. Hu, R. Y. F. Liu, D. A. Schiraldi, A. Hiltner and E. Baer, *Macromolecules*, 2004, **37**, 2136-2143.
41. P. J. Flory, *Proceedings of the Royal Society of London. Series A, Mathematical and Physical Sciences*, 1956, **234**, 73-89.
42. *Ticona: Technical Data Sheet*, 2001.

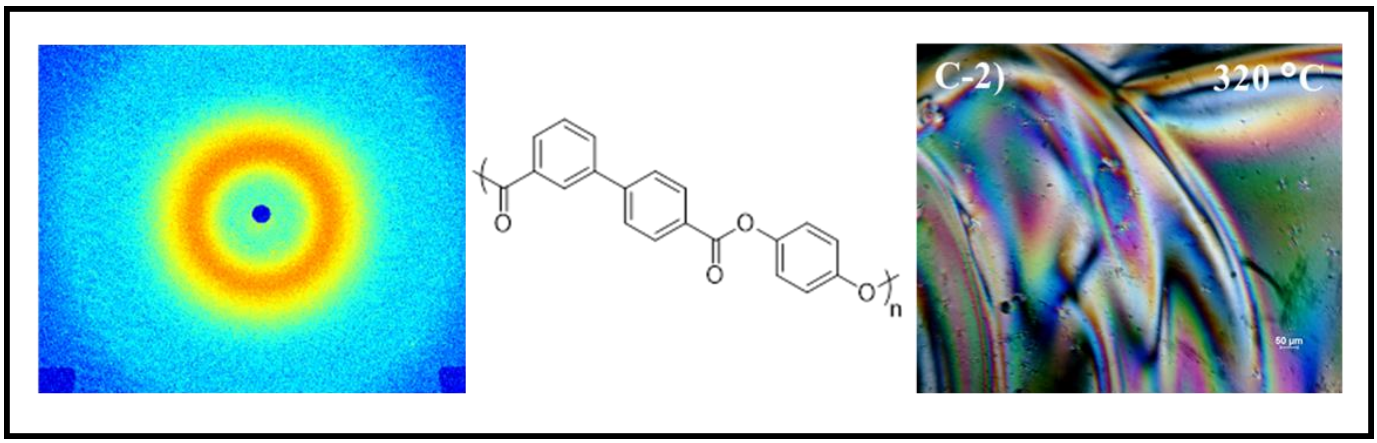

Fully-aromatic homopolyester based on biphenyl 3,4’-bibenzoate facilitates nematic mesophase and restricted crystallization.